J. Math. Biol. (2010) 61:207–229
DOI 10.1007/s00285-009-0296-1

Mathematical Biology

Synchronized oscillation of the segmentation clock gene in vertebrate development

Koichiro Uriu · Yoshihiro Morishita · Yoh Iwasa

Received: 13 July 2008 / Revised: 4 August 2009 / Published online: 16 September 2009

Abstract In vertebrate somitogenesis, "segmentation clock" genes (*her* in zebrafish, *hes* in mouse, and *hairy* in chick) show oscillation, synchronized over nearby cells through intercellular interaction. In zebrafish, neighboring cells interact by Delta-Notch signaling to realize synchronization. Under Delta-Notch, however, a cell with a high expression of the segmentation clock gene tends to suppress its expression in adjacent cells, which might produce spatial heterogeneity instead of synchronized oscillation. Here we studied the conditions under which pre-somitic mesoderm cells show synchronized oscillation of gene expression mathematically. We adopted a model that explicitly considers the kinetics of the mRNA and proteins of the segmentation clock gene and cell–cell interaction via Delta-Notch signaling. From statistical study of a model with randomly generated parameters, we revealed how the likelihood that the system generates stable synchronized oscillation depends on the rate of each reaction in the gene–protein kinetics.

Keywords Somitogenesis · Zebrafish · Synchronization · Segmentation clock gene

Mathematics Subject Classification (2000) 92C15

K. Uriu (✉) · Y. Morishita · Y. Iwasa
Department of Biology, Faculty of Sciences, Kyushu University,
Fukuoka 812-8581, Japan
e-mail: uriu@bio-math10.biology.kyushu-u.ac.jp

Y. Morishita
PRESTO Japan Science and Technology Agency, 4-1-8 Honcho Kawaguchi,
Saitama 332-0012, Japan

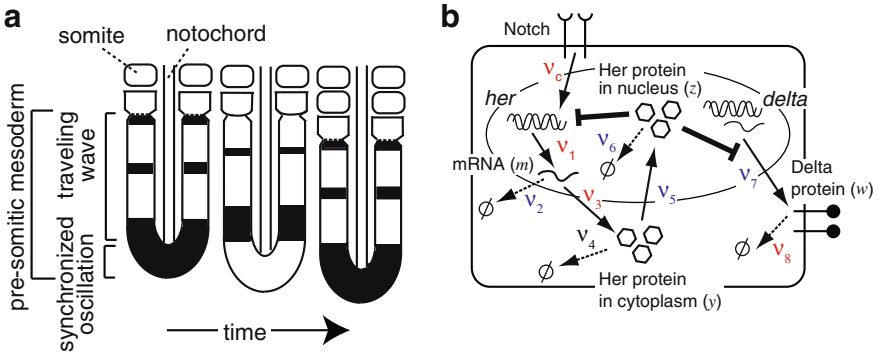

Fig. 1 **a** Expression pattern of the *her* gene in the zebrafish pre-somitic mesoderm. *Black* indicates regions with high gene expression. Anterior is at the *top* and posterior at the *bottom*. **b** Negative feedback regulation of the *her* gene in a cell and intercellular interaction between neighboring cells via Delta-Notch signaling. Production, activation, and transport are represented by *arrows*, whereas suppression is shown as a line ending with a *perpendicular bar*. Decay of mRNA and proteins is denoted by an *arrow* leading to the symbol Ø. *Red* (*blue*) parameters are those for which larger (smaller) values favor stable synchronized oscillation. Neither larger nor smaller values of ν_4 favor stable synchronized oscillation

1 Introduction

Diverse spatio-temporal patterns are generated if many oscillators are arranged spatially and coupled with each other locally (Kobayashi et al. 2006; Kuramoto 1984; Winfree 2000; Wu and Yamaguchi 2004). This has been shown not only in physics and neurophysiology but also in developmental biology. An example is the traveling wave of expression of the segmentation clock gene that appears during vertebrate somite formation.

In vertebrate development, somites bud off from the anterior end of the pre-somitic mesoderm one by one. The time interval between the formation of one unit and the next is species-specific. Underlying this periodic formation of somites are genes that show oscillatory expression in the pre-somitic mesoderm (Bessho et al. 2001; Holley et al. 2000; Jouve et al. 2000; Oates and Ho 2002; Palmeirim et al. 1997). Timing of the segmentation is considered to be controlled by the expression of these segmentation clock genes because their period of oscillation is very close to that of segmentation. In the posterior region of the pre-somitic mesoderm, the oscillatory expression of these genes is synchronized among neighboring cells, and this synchronization is achieved by cell–cell contact (Maroto et al. 2005; Masamizu et al. 2006). In the anterior region of the pre-somitic mesoderm, the segmentation clock genes exhibit a wave-like expression pattern: the region with high gene expression moves anteriorly with time (Fig. 1a). The molecular mechanism generating oscillatory expression of the segmentation clock genes is negative feedback regulation by their own products (Giudicelli et al. 2007; Hirata et al. 2002; Holley et al. 2002; Horikawa et al. 2006).

Theoretical models of segmentation in vertebrates have been developed to explain the spatio-temporal periodicity of the segmentation process (Baker et al. 2006; Collier et al. 2000; Cooke and Zeeman 1976; Kerszberg and Wolpert 2000; Meinhardt 1982, 1986), the oscillatory expression of the segmentation clock genes (Cinquin 2007;

Goldbeter and Pourquie 2008; Lewis 2003; Rodriguez-Gonzalez et al. 2007; Barrio et al. 2006), the wave-like gene expression (Cinquin 2007; Jaeger and Goodwin 2002; Kaern et al. 2000; Tiedemann et al. 2007; Uriu et al. 2009), and the synchronization between cells (Horikawa et al. 2006; Lewis 2003; Tiedemann et al. 2007).

Both oscillation and synchronization of clock gene expression are necessary for normal segmentation. Disruption of the synchronization results in a defective somite boundary (Ozbudak and Lewis 2008; Riedel-Kruse et al. 2007). In zebrafish, the synchronization is realized by intercellular interaction via Delta-Notch signaling (Horikawa et al. 2006; Ozbudak and Lewis 2008; Riedel-Kruse et al. 2007; Jiang et al. 2000; Mara et al. 2007). Previously developed computer simulation models have shown that Delta-Notch signaling can successfully lead to synchronized oscillation among cells (Horikawa et al. 2006; Lewis 2003; Tiedemann et al. 2007). However, we would like to note that it is not obvious how synchronized oscillation is achieved by Delta-Notch signaling. Delta proteins in a cell stimulate expression of the *her* clock gene in neighboring cells via a receptor called Notch, but the active expression of *her* in these cells results in suppression of the *delta* gene within them (Giudicelli et al. 2007; Horikawa et al. 2006). Hence, a cell actively expressing *delta* can suppress *delta* gene expression in its neighbors, possibly maintaining differences between the cells. In fact, Delta-Notch is responsible for the checkerboard pattern of insect neurogenesis (Collieret al. 1996; Honda et al. 1990, 2000; Tanemura et al. 1991), which suggests that synchronization of neighboring cells might be difficult. Hence, we need to examine more carefully how synchronization between neighboring cells can be realized by Delta-Notch signaling in the case of *her* oscillation in the zebrafish pre-somitic mesoderm.

In this paper, we study the mathematical conditions under which synchronized oscillation of *her* gene expression is realized by cell–cell interaction via Delta-Notch signaling. We adopt models that explicitly consider the kinetics of mRNA and proteins for different states (Fig. 1b). To make analytical treatment possible, we first focus on a two-cell system and later study an N-cell system in one and two dimensions. We perform a stability analysis of a limit cycle in which cells are perfectly synchronized. From statistical analysis of the results with randomly chosen parameters, we show that synchronized oscillation tends to be stable, for example, if the production of Delta protein and the degradation of *her* mRNA are slow, and if the transcription of *her* mRNA, the translation of Her protein, and the degradation of Delta protein are fast.

2 Model of gene–protein kinetics in a cell

Mathematical models of cell–cell interactions mediated by membrane proteins have been proposed previously in insect neurogenesis (Collieret al. 1996; Honda et al. 1990, 2000; Tanemura et al. 1991), epidermal wound healing (Owen and Sherratt 1998; Rudge and Burrage 2008), and vertebrate somitogenesis. Some previous studies of vertebrate somitogenesis used models with a time delay in order to generate the oscillatory expression of the segmentation clock genes (Horikawa et al. 2006; Cinquin 2007; Lewis 2003; Rodriguez-Gonzalez et al. 2007; Barrio et al. 2006), but others used a model that explicitly considered the processes in the cell responsible for time delays

such as transport of a protein from cytoplasm to nucleus (Tiedemann et al. 2007; Uriu et al. 2009). In the present study, we adopt simple kinetics in which the mRNA and the protein in cytoplasm and the protein in nucleus are explicitly considered, without assuming a time delay (Fig. 1b).

Each cell is identified by index $i (i = 1, 2, .., N)$. Let m_i, y_i, z_i, and w_i be the concentrations of *her* mRNA, Her protein in cytoplasm, Her protein in nucleus, and Delta protein in cell i, respectively. We assume that all cells have the same values of reaction parameters. The following equation describes the kinetics in cell i :

$$\frac{dm_i}{dt} = \frac{K_1^n}{K_1^n + z_i^n}\left(\nu_1 + \nu_c \hat{w}_i\right) - \frac{\nu_2 m_i}{K_2 + m_i}, \tag{1a}$$

$$\frac{dy_i}{dt} = \nu_3 m_i - \frac{\nu_4 y_i}{K_4 + y_i} - \nu_5 y_i, \tag{1b}$$

$$\frac{dz_i}{dt} = \nu_5 y_i - \frac{\nu_6 z_i}{K_6 + z_i}, \tag{1c}$$

$$\frac{dw_i}{dt} = \nu_7 \frac{K_7^h}{K_7^h + z_i^h} - \frac{\nu_8 w_i}{K_8 + w_i}, \text{(for } i = 1, 2, \ldots, N). \tag{1d}$$

Equation (1a) describes the time evolution of *her* mRNA. The first term represents the transcription of *her* mRNA. ν_1 is the basal transcription rate, and ν_c is the activation rate by Delta-Notch signaling, where Delta is the ligand of the Notch receptor. We assume that Delta-Notch signaling received from neighboring cells is equal to the average abundance of Delta protein among neighbors, denoted by $\hat{w}_i$. The specific form of $\hat{w}_i$ depends on the number of neighboring cells. Her protein in nucleus, z_i (in the denominator), suppresses the transcription of its own gene. We use a Hill-type function to describe this repression. The second term represents the degradation of *her* mRNA.

Equation (1b) describes the time evolution of Her protein in cytoplasm. The first term represents the synthesis of Her protein by translation. The second term represents its degradation. Equation (1c) describes the time evolution of Her protein in nucleus. The first term of Eq. (1c) represents the transport of Her protein from the cytoplasm to the nucleus, while the third term of Eq. (1b) represents the decrease of Her protein in cytoplasm as a result of this transport. The second term of Eq. (1c) represents the degradation of the protein in the nucleus. We assume a Michaelis-Menten type reaction for the degradation of *her* mRNA and Her protein, since degradation is an enzymatic process, as has been shown for Hes1 protein in mouse embryo (Hirata et al. 2002). Kurosawa and Iwasa (2002) proved that strong saturation of mRNA and protein degradation promotes the oscillation of circadian clock gene expression. They demonstrated that most published models and simulators of the circadian clock and of the mitotic oscillator have strongly saturated rate functions for the degradation of mRNA and proteins. In addition, a previous model of the segmentation clock gene in mouse also assumed saturating functions for the degradation of mRNA and protein (Goldbeter and Pourquie 2008).

Equation (1d) describes the time evolution of Delta proteins, which are expressed on the cell membrane. The first term represents the synthesis of Delta protein. Her

protein suppresses Delta protein synthesis by inhibiting *delta* mRNA transcription (Giudicelli et al. 2007; Horikawa et al. 2006). The second term represents Delta protein degradation.

Equation (1) is a simple model for describing the regulation of *her* gene expression. We also analyzed a more detailed model including the time evolution of *delta* mRNA explicitly. We confirmed that the detailed model gave similar results to those yielded by the model described by Eq. (1). To keep the logic clearer, we focus on Eq. (1) in the main text of this paper, and summarize the results of the detailed model in Appendix B.

Parameter values

The permitted range of each parameter used in this study is listed in Table 1. The *her* mRNA transcription rate was chosen to lie between 0.4 and 40 copies per minute and the translation rate of Her protein was chosen to lie between 0.5 and 50 copies per minute per mRNA copy for a cell with a diameter of 10 μm (cell volume, 524 μm^3) (Cinquin 2007). The ranges of the Michaelis constants and of the maximum degradation rates of mRNA and proteins are based on those given by Goldbeter and Pourquie (2008). The values of the Hill coefficients (n and h) are determined by the dimerization processes of Her proteins and the number of Her protein binding sites on DNA (Zeiser et al. 2007). However, details are not known yet. Hence, we analyzed the model with Hill coefficient values of one, two, three, and four. Below we describe the results for the system with a Hill coefficient value set to two, and we briefly summarize the results for systems with different Hill coefficient values in Sect. 3.3.1.

3 Results

3.1 Perfectly synchronized oscillation of segmentation clock genes

Our focus here is on the stability of synchronized oscillation among all N cells in the pre-somitic mesoderm. The synchronized oscillation corresponds to a limit cycle of the equation obtained by setting $m = m_1 = \cdots = m_N$, $y = y_1 = \cdots = y_N$, $z = z_1 = \cdots = z_N$, and $w = w_1 = \cdots = w_N$ in Eq. (1). Because $\hat{w}_i$ in Eq. (1) is the average concentration of Delta protein expressed by neighboring cells, we obtain the following four-variable equation:

$$\frac{dm}{dt} = \frac{K_1^n}{K_1^n + z^n}(\nu_1 + \nu_c w) - \frac{\nu_2 m}{K_2 + m}, \tag{2a}$$

$$\frac{dy}{dt} = \nu_3 m - \frac{\nu_4 y}{K_4 + y} - \nu_5 y, \tag{2b}$$

$$\frac{dz}{dt} = \nu_5 y - \frac{\nu_6 z}{K_6 + z}, \tag{2c}$$

$$\frac{dw}{dt} = \nu_7 \frac{K_7^h}{K_7^h + z^h} - \frac{\nu_8 w}{K_8 + w}. \tag{2d}$$

Table 1 Ranges from which parameters were selected

Parameter	Definition	Range and units	Values used for Fig. 3
ν_1	Basal transcription rate of *her* mRNA	0.001–0.1 nM min^{-1}	(a) 0.069, (b) 0.001, (c) 0.089, (d) 0.006
ν_2	Maximum degradation rate of *her* mRNA	0.1–10 nM min^{-1}	(a) 0.963, (b) 0.665, (c) 0.105, (d) 1.92
ν_3	Translation rate of Her protein	0.5–50 min^{-1}	(a) 1.172, (b) 7.486, (c) 5.719, (d) 4.088
ν_4	Maximum degradation rate of Her protein in cytoplasam	0.1–10 nM min^{-1}	(a) 1.447, (b) 9.389, (c) 3.471, (d) 0.495
ν_5	Cytoplasm-nucleus transportation rate of Her protein	0.01–1.0 min^{-1}	(a) 0.076, (b) 0.288, (c) 0.045, (d) 0.344
ν_6	Maximum degradation rate of Her protein in nucleus	0.1–10 nM min^{-1}	(a) 0.147, (b) 0.769, (c) 0.699, (d) 1.519
ν_7	Synthesis rate of Delta protein	0.1–10 nM min^{-1}	(a) 1.912, (b) 0.128, (c) 1.217, (d) 3.876
ν_8	Maximum degradation rate of Delta protein	0.1–10 nM min^{-1}	(a) 2.315, (b) 0.628, (c) 2.772, (d) 8.521
ν_c	Activation rate of *her* mRNA transcription by Delta-Notch signal	0.01–1.0 min^{-1}	(a) 0.708, (b) 0.894, (c) 0.076, (d) 0.483
K_1	Threshold constant for the suppression of *her* mRNA transcription by Her protein	0.1–10 nM	(a) 0.103, (b) 4.753, (c) 0.497, (d) 2.152
K_2	Michaelis constant for *her* mRNA degradation	0.1–10 nM	(a) 9.916, (b) 0.983, (c) 0.128, (d) 8.658
K_4	Michaelis constant for Her protein degradation in cytoplasm	0.1–10 nM	(a) 0.182, (b) 0.783, (c) 3.732, (d) 0.395
K_6	Michaelis constant for Her protein degradation in nucleus	0.1–10 nM	(a) 0.302, (b) 0.163, (c) 0.357, (d) 0.436
K_7	Threshold constant for the suppression of Delta protein synthesis by Her protein	0.1–10 nM	(a) 1.87, (b) 0.936, (c) 0.156, (d) 9.901
K_8	Michaelis constant for Delta protein degradation in nucleus	0.1–10 nM	(a) 0.377, (b) 5.065, (c) 3.7, (d) 8.271

In order to examine the (local) stability, we need to find a limit cycle solution for Eq. (2). To do so, we first performed a linear stability analysis of the equilibrium of Eq. (2) with each parameter set to a randomly chosen value within the ranges shown in Table 1, and checked whether the Eq. (2) with that parameter set could have limit cycles (see Appendix A for details). If the model had an unstable equilibrium, we solved the differential equations numerically and searched for limit cycles with a period of 25–35 min, because the period of oscillation of *her* gene expression in zebrafish somitogenesis is about 30 min (Saga and Takeda 2001). Subsequently, we

solved Eq. (2) for different initial conditions to check whether the limit cycle with a period of 25–35 min was the only attractor of the constrained model Eq. (2). To prepare these initial conditions, we first calculated the time average of each variable in the limit cycle. Then, we chose an initial value of each variable from among the time average, the time average $\times 10$, and the time average $/10$. Because the model has four variables, we had $3^4 = 81$ sets of initial conditions. When a limit cycle was found in this manner, it was almost always the only attractor in Eq. (2) (82.4% of 10,000 limit cycles having a period of 25–35 min). Note that a limit cycle in Eq. (2) is also a limit cycle in the full system of Eq. (1), but it may or may not be stable in Eq. (1). In the following analysis, we focus on the parameter sets that generated a single limit cycle in Eq. (2).

We studied the parameter dependence of the period of oscillation of limit cycles found in this manner. Since the period determines both the timing of segmentation and the length of each somite (Cooke and Zeeman 1976; Saga and Takeda 2001; Dubrulle and Pourquie 2002), it is useful to know how the period of oscillation depends on the parameter values. We sampled a parameter set that could generate a limit cycle satisfying the above conditions, and then we increased a focal parameter by 10% while holding all other parameters fixed and calculated the relative change in the period of oscillation. We repeated this procedure many times (about 1,200). Figure 2a shows, for example, the dependence of the period on the degradation rate of *her* mRNA (ν_2) and on the synthesis rate of Delta protein (ν_7).

We applied this procedure to each parameter. Results for the parameter sensitivity of the period are shown in Fig. 2b. We calculated the fraction of runs in which an increase (decrease) of the period was observed (indicated by the black (white) bar in Fig. 2b). Figure 2c and d show the relative change in the period of oscillation. The period of oscillation strongly increased when the synthesis rate of Delta protein (ν_7) was increased. Increases in the transcription activation rate by Delta-Notch signaling (ν_c), the threshold constant for inhibition of *her* mRNA transcription by Her protein (K_1), that for inhibition of Delta protein synthesis by Her protein (K_7), the Michaelis constant for *her* mRNA degradation (K_2), and the Michaelis constant for Delta protein degradation (K_8) also lengthened the period of oscillation, but their influences were relatively small (Fig. 2b, c).

In contrast, the period of oscillation clearly decreased with increases in the degradation rate of *her* mRNA (ν_2), the cytoplasm–nucleus transport rate of Her protein (ν_5), and the degradation rate of Delta protein (ν_8) (Fig. 2b, d). Increases in the translation rate of Her protein (ν_3) and the Michaelis constant for Her protein degradation in cytoplasm (K_4) and nucleus (K_6) also shortened the period, but their influences were relatively small (Fig. 2b, d).

Increases in the basal transcription rate of *her* mRNA (ν_1) and the degradation rate of Her protein in cytoplasm (ν_4) and nucleus (ν_6) lengthened or shortened the period of oscillation, depending on the values of the other parameters (Fig. 2b).

3.2 Stability analysis of perfectly synchronized oscillation

Once we obtain a limit cycle, its local stability can be examined by linearizing the dynamics Eq. (1) along the limit cycle. To illustrate this analysis, we first consider

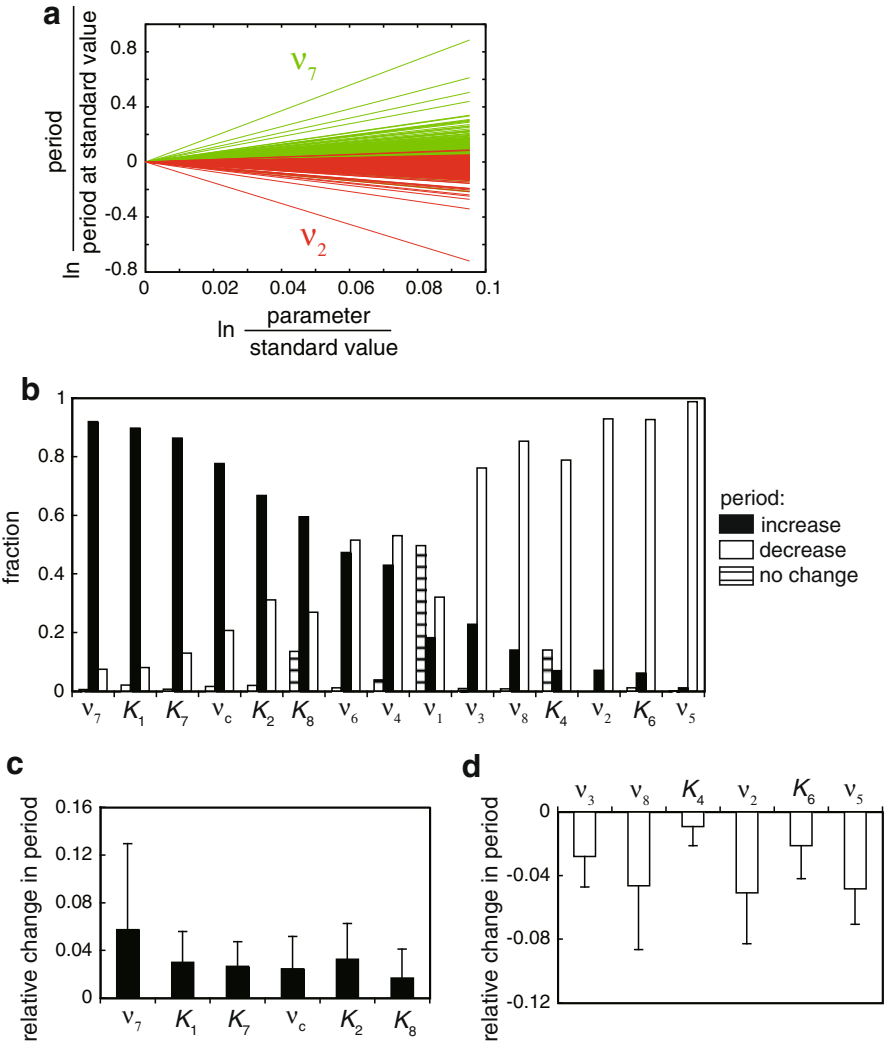

Fig. 2 **a** Dependence of the period of oscillation on the degradation rate of *her* mRNA (ν_2 (*red*) and on the synthesis rate of Delta protein (ν_7 (*green*). We sampled 1,239 parameter sets and calculated the period of oscillation. Then we increased ν_2 or ν_7 by 10% from the original value and re-examined the period. All results are plotted. **b** Fraction of parameter sets showing a change in the period of oscillation when each parameter was increased by 10% from the standard value. "No change" means that we did not observe any change in the period. **c** and **d** Change in the period of oscillation for shifted parameters relative to the period with the standard parameter set. The average and the SD are shown. In **b**–**d**, we calculated the fraction and the average only for those cases in which a limit cycle existed even when the focal parameter was shifted as in **a**. For each parameter, about 94% of 1,239 parameter sets kept the limit cycle

the case of two cells ($N = 2$). As we show later, the parameter dependence of the stability of the synchronized oscillation is very similar between a two-cell system and systems with larger N. Therefore, detailed analysis of this simplest case is useful for understanding more realistic cases.

The system is described by eight variables, and the intercellular interaction term $\hat{w}_i$ in Eq. (1a) becomes $\hat{w}_1 = w_2$ and $\hat{w}_2 = w_1$ respectively. Let $\boldsymbol{\phi}(t) = (m(t), y(t), z(t), w(t), m(t), y(t), z(t), w(t))^{\mathrm{T}}$ be a limit cycle in which the two cells are perfectly synchronized. $\boldsymbol{\phi}(t) = \boldsymbol{\phi}(t+T)$, where T is the period of oscillation. Let $\tilde{\mathbf{x}} = (\tilde{m}_1, \tilde{y}_1, \tilde{z}_1, \tilde{w}_1, \tilde{m}_2, \tilde{y}_2, \tilde{z}_2, \tilde{w}_2)^{\mathrm{T}}$ represent a small deviation from this limit cycle. We linearized Eq. (1) around the limit cycle $\boldsymbol{\phi}(t)$ and derived the following linear differential equation with periodic coefficients:

$$\frac{d\tilde{\mathbf{x}}}{dt} = D\mathbf{f}(\boldsymbol{\phi})\,\tilde{\mathbf{x}}, \tag{3a}$$

where the matrix $D\mathbf{f}(\boldsymbol{\phi})$ is given by:

$$D\mathbf{f}(\boldsymbol{\phi}) = \begin{pmatrix} A & B \\ B & A \end{pmatrix}, \tag{3b}$$

where

$$A = \begin{pmatrix} -\frac{\nu_2 K_2}{(K_2+m(t))^2} & 0 & -\frac{K_1^n n z(t)^{n-1}(\nu_1+\nu_c w(t))}{\left(K_1^n+z(t)^n\right)^2} & 0 \\ \nu_3 & -\frac{\nu_4 K_4}{(K_4+y(t))^2} - \nu_5 & 0 & 0 \\ 0 & \nu_5 & -\frac{\nu_6 K_6}{(K_6+z(t))^2} & 0 \\ 0 & 0 & -\frac{\nu_7 K_7^h h z(t)^{h-1}}{\left(K_7^h+z(t)^h\right)^2} & -\frac{\nu_8 K_8}{(K_8+w(t))^2} \end{pmatrix}, \tag{3c}$$

$$B = \begin{pmatrix} O & C \\ O & O \end{pmatrix}, \quad C = \begin{pmatrix} 0 & \frac{\nu_c K_1^n}{K_1^n+z(t)^n} \\ 0 & 0 \end{pmatrix}. \tag{3d}$$

Let $\tilde{\mathbf{x}}_i(t)$ be the solution of Eq. (3) for the initial condition $\tilde{\mathbf{x}}_i(0) = \mathbf{e}_i.\mathbf{e}_i$ is a vector whose ith element is 1, all others being 0. Then the 8×8 matrix $F(t) = (\tilde{\mathbf{x}}_1(t), \tilde{\mathbf{x}}_2(t), .., \tilde{\mathbf{x}}_8(t))$ is called the fundamental solution matrix (Niwa 1995).

Let $\delta\mathbf{x}_0$ be a small deviation from the limit cycle at a certain time point. The change in the deviation after one period of the limit cycle is described by the following equation (Niwa 1995):

$$\delta\mathbf{x}(T) = F(T)\,\delta\mathbf{x}_0, \tag{4}$$

where T is the period of the limit cycle. The stability of a limit cycle is determined by the eigenvalues of this fundamental solution matrix. If the matrix $F(T)$ has an eigenvalue with absolute value larger than unity, the deviation grows with time and the limit cycle is unstable.

The synchronized oscillation may be stable or unstable. Figure 3a shows an example of stable synchronized oscillation in the two-cell system. If when the cells in this system showed synchronized oscillation, we shifted the phase of the oscillation (by 10%

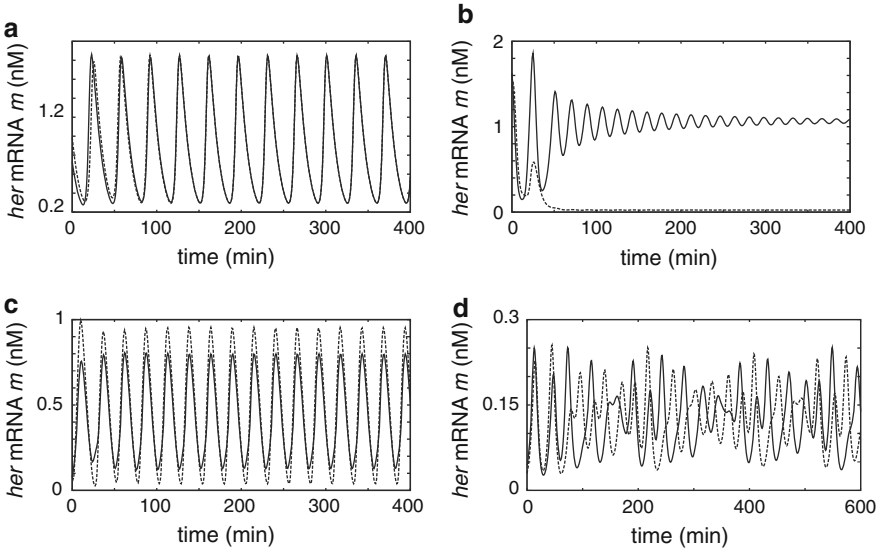

Fig. 3 **a**–**d** Examples of expression patterns in the two-cell system ($N = 2$). The *horizontal axis* is time, and the *vertical axis* is the concentration of *her* mRNA. We changed the variables of one cell along the limit cycle, and set the other cells to show a phase difference of 10% of the period at $t = 0$. Parameter values used for each panel are given in Table 1. $n = h = 2$ in Eq. (1). **a** Stable synchronized oscillation, **b** heterogeneous expression pattern, **c** oscillatory expression pattern with different amplitudes and phases between the cells, and **d** irregularly oscillatory expression pattern

of the period) by changing the variables along the limit cycle, the trajectory returned to the limit cycle with the two cells perfectly synchronized. This result confirms that Delta-Notch signaling is able to synchronize the oscillatory expression of the *her* gene between cells given appropriate parameters.

Figure 3b–d show examples of expression patterns when the synchronized oscillation is unstable in the two-cell system. In these examples, if we shifted the phase of the oscillation between the cells in the same way as in the example shown in Fig. 3a, the difference in the variables in Eq. (1) grew with time and the cells left the synchronized state. In the example shown in Fig. 3b, the oscillation of gene expression damps in both cells, which begin to show spatially heterogeneous stationary expression of the *her* gene. A similar spatial heterogeneity of gene expression between the cells is generated by Delta-Notch signaling during peripheral nervous system formation in insects (Collieret al. 1996; Honda et al. 1990, 2000; Tanemura et al. 1991). Figure 3c shows asynchronous oscillatory expression in which the phase and amplitude of oscillation differ between the cells. In Fig. 3d, the cells show irregularly oscillatory gene expression.

3.3 Parameter dependence of the stability conditions

Since the model includes a large number of parameters, examining the stability conditions for synchronized oscillation and summarizing the results in a useful manner is not

very easy. In addition, at this moment, experimental identification of exact parameter values for the segmentation clock gene reactions is not possible. Hence, we analyzed the parameter dependence of stability by examining the fraction of runs resulting in stable synchronized oscillation among all runs of systems with randomly generated parameters.

We first generated 8,238 sets of parameters that could produce a single limit cycle in Eq. (2) using the procedures explained in Sect. 3.1. The logarithmic values of each parameter were distributed uniformly within its range, given in Table 1. Then, we examined the linear stability of these limit cycles in the full system given by Eq. (1). To examine the parameter dependence of the limit cycle stability, we divided the parameter range into two intervals and compared the stable limit cycle fractions between them. For example, to examine the effect of parameter ν_2 on the likelihood that the limit cycle would be stable, we compared the fraction of runs with a stable limit cycle when the parameter value was small (ν_2 between 0.1 and 1) with that when it was large (ν_2 between 1 and 10). If the fraction of parameter sets with a stable limit cycle was greater when the parameter value was large than when it was small, we then concluded that a larger value of the focal parameter tended to promote the stability of the limit cycle. If the opposite was true, we concluded that a smaller value of the focal parameter promoted the stability of the limit cycle. Similarly, we compared the fraction of parameter sets with a stable limit cycle when each parameter was small or large. In this procedure, we separated the parameter's range into two intervals by using the geometric average of the upper and lower limits of the range (e.g., $1 = \sqrt{0.1 \times 10}$ in the case of ν_2). We confirmed that the trend of the parameter dependence of stability was very similar when we divided each parameter range into 4–10 intervals and analyzed the data in the same way.

3.3.1 Two-cell system

Among the 8,238 parameter sets that generated a limit cycle with two cells perfectly synchronized (synchronized oscillation) in Eq. (1), the synchronized oscillation was stable with 683 parameter sets (8.3%), whereas it was unstable with the other 7,555 sets (91.7%) (Fig. 4a). Figure 4b shows the fractions of runs resulting in stable synchronized oscillation for large (black bar) and small (white bar) parameter values. The difference between these two fractions was statistically significant for all parameters except for the degradation rate of Her protein in cytoplasm (ν_4) (1% significance level by chi-square test).

For the basal transcription rate of *her* mRNA (ν_1), the translation rate of Her protein (ν_3), the degradation rate of Delta protein (ν_8), the activation rate of *her* mRNA transcription by Delta-Notch signaling (ν_c), the Michaelis constant for *her* mRNA degradation (K_2), the threshold constant for the suppression of Delta protein synthesis by Her protein (K_7), and the Michaelis constant for Delta protein degradation (K_8), the fraction with stable synchronized oscillation was larger when the parameter values were large than when they were small (Fig. 4b). This suggests that larger values of these parameters promote synchronized oscillation of the system.

Next, we examined the likelihood of generating stable synchronized oscillation when we combined results, shown in Fig. 4b, obtained from the analyses of single

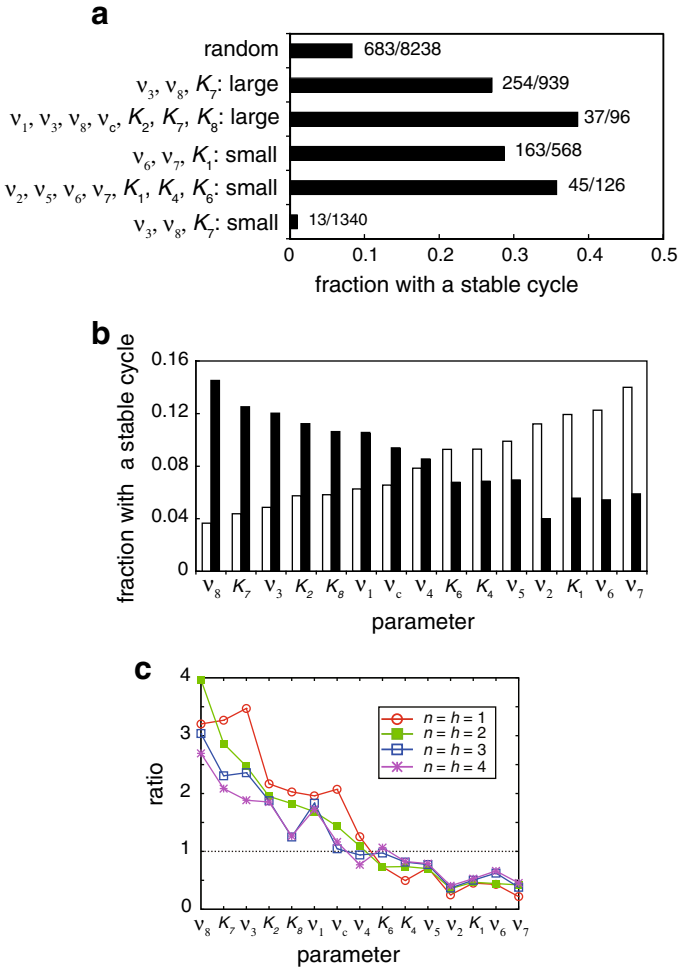

Fig. 4 **a** Fractions of parameter sets showing stable synchronized oscillation. **b** Fractions showing stable synchronized oscillation when the focal parameter was large (*black bar*) and when it was small (*white bar*). Results for the system with a Hill coefficient of two ($n = h = 2$ in Eq. (1)). **c** Results for systems with Hill coefficients of one (*circles*), two (*filled squares*), three (*open squares*), or four (*crosses*). The *vertical axis* shows the ratio of the fractions showing stable synchronized oscillation when the focal parameter was large to the fractions showing stable synchronized oscillation when it was small. In **a**–**c**, $N = 2$

parameters. For example, when all of ν_3, ν_8, and K_7 were large, the fraction with stable synchronized oscillation was 27.0% (in contrast, when all of these parameters were small, the synchronized oscillation was always unstable) (Fig. 4a). Furthermore, when all of the parameters that when large individually promoted synchronized oscillation were large, the fraction with stable synchronized oscillation was 38.5% (Fig. 4a); this value is much larger than that of 8.3% obtained when all of the parameters were chosen randomly from the ranges listed in Table 1. Thus, Eq. (1) is much more likely to generate stable synchronized oscillation when the results obtained from the analyses of single parameters (Fig. 4b) are combined.

Smaller values of the *her* mRNA degradation rate (ν_2), the transport rate of Her protein (ν_5), the degradation rate of Her protein in nucleus (ν_6), the synthesis rate of Delta protein (ν_7), the threshold constant for the suppression of *her* mRNA transcription by Her protein (K_1), and the Michaelis constants for Her protein degradation in cytoplasm (K_4) and nucleus (K_6) promoted stable synchronized oscillation (Fig. 4b). When all of ν_6, ν_7, and K_1 were small, the fraction of stable synchronized oscillation was 28.7% (Fig. 4a). Further, when all of the parameters that when small individually promoted synchronized oscillation were small, the fraction of stable synchronized oscillation was 35.7% (Fig. 4a).

We confirmed that the unstable synchronized oscillations shown in Fig. 3b–d became stable when some parameter values were shifted from those used for Fig. 3b–d in ways that accorded with the above results. For example, if we decreased the value of K_1 and increased the value of K_7 from the values used for Fig. 3b, keeping the other parameter values fixed, the synchronized oscillation became stable, as our stability analysis predicted.

We also examined the dependence of stability on parameters when different values were used for the Hill coefficients ($n = h = 1, 3$, and 4 in Eq. (1)). In Fig. 4c, for each parameter we plotted the ratio of fractions with stable synchronized oscillation when the focal parameter was large to fractions with stable synchronized oscillation when it was small. As the Hill coefficient increased, the stability dependence on several parameters, such as ν_3, ν_c, K_4, K_6, K_7, and K_8, became weaker compared with when the Hill coefficient was smaller (Fig. 4c). However, the parameter dependence of the fraction having stable synchronized oscillation was similar for all Hill coefficient values.

To conclude, the speed of certain reactions should be fast (slow) for Eq. (1) to be likely to produce stable synchronized oscillation.

3.3.2 N cells aligned linearly

Next, we examined the situation where N cells were linearly aligned (Fig. 5a). In this case, $\hat{w}_i$ in Eq. (1a) becomes the average of the Delta protein concentration in the left and the right neighbors ($i - 1$ and $i + 1$) of cell i. For cells at the two ends, $\hat{w}_i$ is the Delta protein concentration in their single neighbor.

As the cell number increases, it takes much more computational time to calculate the fundamental solution matrix and its eigenvalues (the size of the matrix is $4N \times 4N$). As a result, the linear stability analysis described above becomes difficult to apply when the cell number N is large. In the present study, we performed a detailed analysis of cases with a relatively small cell number N ($N = 4, 6,$ and 8), using many different parameter sets. We examined cases when the Hill coefficient was equal to two ($n = h = 2$ in Eq. (1)).

We applied the same analysis that we employed in the two-cell case. The results for the two-cell system overlapped greatly with results for systems with four, six, or eight cells aligned linearly (Fig. 5c), suggesting that the results derived from the two-cell system still hold for N cells aligned linearly.

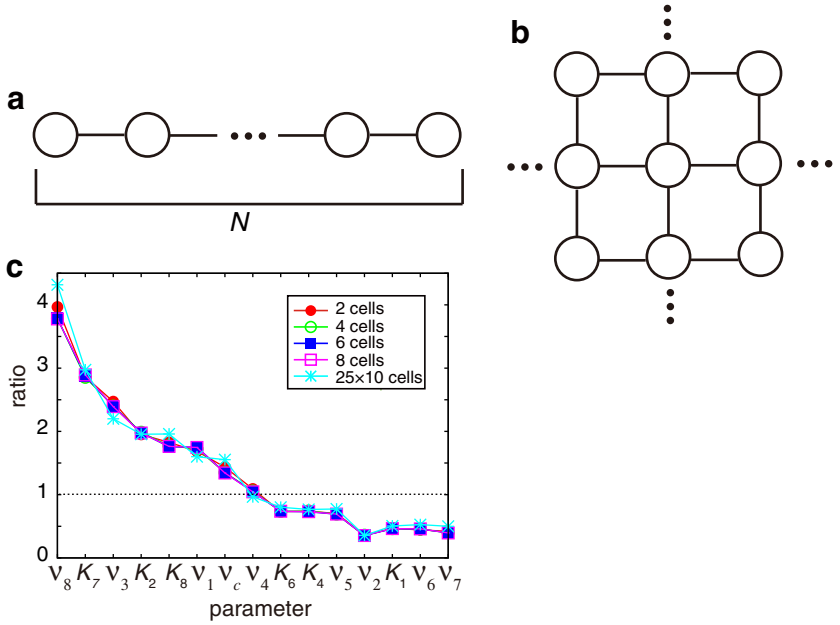

Fig. 5 **a** N cells aligned linearly, and **b** N cells in a two-dimensional square lattice. **c** The results for systems with $N = 2$ (*red filled circles*), 4 (*green open circles*), 6 (*blue filled squares*), and 8 (*pink open squares*), all linearly aligned, and for a system with $N = 25 \times 10$ (two-dimensional lattice; *light blue crosses*). $n = h = 2$ in Eq. (1). The vertical axis is the ratio of fractions showing stable synchronized oscillation when the focal parameter was large to the fractions showing stable synchronized oscillation when it was small. For each value of N, we examined 8,238 limit cycles with the cells perfectly synchronized

3.3.3 N cells in a two-dimensional lattice

As a more realistic description of the pre-somitic mesoderm, we also considered the case in which the cells are arranged in a two-dimensional square lattice (Fig. 5b). We consider a rectangular domain of 25×10 cells, which approximates the tailbud region of the pre-somitic mesoderm. Because we adopted a Neumann neighborhood (each cell has four nearest neighbors), $\hat{w}_i$ in Eq. (1a) becomes the arithmetic average of the Delta protein concentrations in the four neighboring cells. For cells on the boundaries, $\hat{w}_i$ is the average in the three or two neighbors.

Because of the large number of cells, we adopted the following criterion for the linear stability of synchronized oscillation, instead of using eigenvalues of the fundamental solution matrix: initially cells were made to show perfectly synchronized oscillation as represented by a limit cycle in Eq. (2). Then we shifted the phase of oscillation of the cells by changing the variables in Eq. (1) along the limit cycle, resulting in a phase difference of up to 1% of the period between cells. If the difference in the time at which cells showed peak *her* mRNA abundance was smaller than 0.1% of the period of synchronized oscillation after 9,000 min, the synchronized oscillation was regarded as stable. We performed a statistical analysis just as for the one-dimensional models studied in the previous sections. We first analyzed the parameter conditions

resulting in stability in the one-dimensional models by both methods—i.e., by calculating the eigenvalues of the fundamental solution matrix around the limit cycle and by examining the phase differences between the cells in a direct numerical simulation. We confirmed that these two methods gave the same results for all of the parameters in Eq. (1) (data not shown).

The results for the two-dimensional model, shown in Fig. 5c, were quite similar to those for the one-dimensional models.

4 Discussion

In this paper, we examined the conditions permitting synchronization of the oscillation of the segmentation clock gene among neighboring cells via Delta-Notch signaling. We adopted a linear stability analysis of the limit cycle and a statistical analysis of a model with randomly generated parameters. We showed which reactions should be fast and which reactions should be slow for the Eq. (1) system to be likely to generate stable synchronized oscillation. An important premise of our paper is that synchronization of the segmentation clock is very important for proper segmentation and hence the parameter values should have evolved to realize and maintain the synchronization robustly. Hence, our conjecture is that the values of rate constants of the kinetics of organisms should be chosen such that they can stabilize the synchronized oscillation, which gives experimentally testable predictions.

By studying both one- and two-dimensional cases, we found that the conditions that enable synchronized oscillation to be achieved depend strongly neither on the total number of cells in a system nor on the number of neighboring cells. This finding suggests that this result might hold in three-dimensional cases as well. When we analyzed a more detailed model than Eq. (1) (Appendix B), for most parameters, we obtained similar results, but with a few differences between one- and two-dimensional systems. We explain these differences as follows: with some parameter sets, the two-dimensional system requires a very long time (more than 9,000 min) to converge to synchronized oscillation. Such synchronized oscillation tends to be regarded as "unstable" owing to the finite calculation period (see Appendix B for details).

In the analyses explained above, we considered only those cases that generated synchronized oscillation with a period close to 30 min (i.e., 25–35 min) when we sampled parameter sets from the ranges listed in Table 1. However, there might be other constraints that we should consider, such as the actual concentrations of molecules at the peak of each oscillation. Thus, we also studied the conditions for achieving stable synchronized oscillation under constraints on both the period of oscillation and the peak concentration of each variable (see Appendix B); we sampled parameter sets for which Eq. (B.1) (Appendix B) resulted in perfectly synchronized oscillation with a period of 25–35 min and with the peak concentration of each variable exceeding 0.1 nM. Under these constraints, the dependence of stability on many parameters remained the same, but the sensitivity of stability to a few parameters changed. Future experimental studies are expected to reveal the actual constraints that we should consider. We do not claim that all possible interesting mathematical behaviors of the Eq. (1) can be captured by our choices of parameter ranges and initial conditions, and we may have missed some

interesting nonlinear behavior of the model. But we do believe that we need to focus our attention on the behaviors of the model that are relevant to biological phenomena and occur over a wide range of parameter values.

In the present paper, we restricted the analyses to a determination of whether the synchronized limit cycle is linearly stable. Investigation of the robustness of the synchronized oscillation to large perturbations (i.e., global stability) is also an important topic for future work. In addition, even if a limit cycle is stable, it may take a very long time to converge after disturbances when the cell–cell interaction is very weak. In zebrafish experiments, the phase of oscillatory gene expression in transplanted cells was quickly (after about three cycles) entrained to that of the cells of the host (Horikawa et al. 2006). It will also be important to study the conditions under which cells can achieve synchronization in a sufficiently short time in future work.

When the number of variables and parameters included in a model are relatively small, we can analyze the model's behavior in detail by using a bifurcation analysis. However, most models in systems biology include ten or more parameters, making such an analysis very difficult. In the present paper, we statistically examined a model with randomly generated parameters. We showed that a statistical approach is a useful way to examine the properties of a model with a large number of parameters and variables.

Many models proposed for segmentation clock genes assume explicit time delays in the negative feedback regulation of the genes (Horikawa et al. 2006; Cinquin 2007; Lewis 2003; Rodriguez-Gonzalez et al. 2007; Barrio et al. 2006). In the present study, we modeled Her protein in cytoplasm and nucleus separately and could generate stable synchronized oscillation without a time delay, as Tiedemann et al. (2007) had done previously. The time delay is caused by the kinetics in the cells, including modification and transport of a molecule, and models having those intermediate states are in effect representing the time delay by multiple variables. Time delay is a handy mathematical expression for an outcome of several different kinetic processes, but explicitly representing the mechanisms that generate the time delay in a model is more useful for determining the biological implications of the model. Furthermore, mathematical stability analysis of limit cycles is much easier in models without a time delay, because a model including a time delay has infinitely many dimensions. Examining whether the conclusions arrived at in this study hold in a system including an explicit time delay, and comparing different models to clarify which are most suitable for generating stable synchronized oscillation of the segmentation clock are interesting problems for future theoretical works.

Acknowledgments This work was done with the support of a Grant-in-Aid from the Japan Society for the Promotion of Science to Y.I. and a PRESTO project of Japan Science and Technology Agency to Y.M. We are grateful to the following people for their very helpful comments: N. Honda, K. Ishimatsu, G. Kurosawa, A.F.M. Marée, A. Mochizuki, R. Schlicht, H. Takeda, H.B. Tiedemann, and Y. Yamaguchi.

Appendix A Stability analysis of the uniform equilibrium

We can calculate the uniform equilibrium m_e, y_e, z_e, and w_e by setting the right-hand sides of Eq. (2) equal to zero. To examine the existence of a uniform equilibrium,

we express m_e, y_e, and w_e as functions of z_e by solving Eqs. (2b), (2c), and (2d). Using these results, we can express Eq. (2a) as an equation that includes only z_e. The first term of Eq. (2a) is a monotonically decreasing function of z_e, whereas the second term, $\nu_2 m_e/(K_2 + m_e)$, is a monotonically increasing function of z_e. We can show that these two functions have an intersection within a range satisfying $m_e > 0, y_e > 0, z_e > 0$, and $w_e > 0$. Hence, Eq. (2) has only one equilibrium.

By using the Taylor expansion and neglecting higher order terms, we obtain the following linear differential equations around the equilibrium of Eq. (2):

$$\frac{d\tilde{m}}{dt} = -A_1\tilde{m} - A_2\tilde{z} + A_3\tilde{w}, \tag{A.1a}$$

$$\frac{d\tilde{y}}{dt} = \nu_3\tilde{m} - B_1\tilde{y}, \tag{A.1b}$$

$$\frac{d\tilde{z}}{dt} = \nu_5\tilde{y} - C_1\tilde{z}, \tag{A.1c}$$

$$\frac{d\tilde{w}}{dt} = -D_1\tilde{z} - D_2\tilde{w}, \tag{A.1d}$$

$$A_1 = \frac{\nu_2 K_2}{(K_2 + m_e)^2}, \quad A_2 = \frac{K_1^n n z_e^{n-1}(\nu_1 + \nu_c w_e)}{(K_1^n + z_e^n)^2}, \quad A_3 = \frac{\nu_c K_1^n}{(K_1^n + z_e^n)},$$
$$B_1 = \frac{\nu_4 K_4}{(K_4 + y_e)^2} + \nu_5, \quad C_1 = \frac{\nu_6 K_6}{(K_6 + z_e)^2}, \quad D_1 = \frac{\nu_7 h z_e^{h-1} K_7^h}{(K_7^h + z_e^h)^2},$$
$$D_2 = \frac{\nu_8 K_8}{(K_8 + w_e)^2}. \tag{A.1e}$$

where $\tilde{m}$, $\tilde{y}$, $\tilde{z}$, and $\tilde{w}$ represent small deviations from equilibrium. We can ascertain the local stability of the equilibrium from the eigenvalues of the Jacobi matrix. After some calculations, we obtain the following characteristic equation:

$$\lambda^4 + \alpha_1\lambda^3 + \alpha_2\lambda^2 + \alpha_3\lambda + \alpha_4 = 0, \tag{A.2a}$$

$$\alpha_1 = A_1 + B_1 + C_1 + D_2, \tag{A.2b}$$

$$\alpha_2 = A_1B_1 + A_1C_1 + B_1C_1 + A_1D_2 + B_1D_2 + C_1D_2, \tag{A.2c}$$

$$\alpha_3 = \nu_3\nu_5A_2 + A_1B_1(C_1 + D_2) + (A_1 + B_1)C_1D_2, \tag{A.2d}$$

$$\alpha_4 = \nu_3\nu_5A_3D_1 + D_2(\nu_3\nu_5A_2 + A_1B_1C_1). \tag{A.2e}$$

Here, $\alpha_1 > 0, \alpha_2 > 0, \alpha_3 > 0$, and $\alpha_4 > 0$ are always satisfied. In accordance with the Routh–Hurwitz condition, all of the eigenvalues have negative real parts and the equilibrium is locally stable if:

$$(\alpha_1\alpha_2 - \alpha_3)\alpha_3 - \alpha_1^2\alpha_4 > 0. \tag{A.3}$$

The equilibrium becomes unstable if inequality (A.3) is violated.

Appendix B Analysis of a more detailed model

We studied a more detailed model that includes the dynamics of the *delta* mRNA concentration explicitly. The results obtained from the analysis (explained below) were quite similar to those obtained from the analysis of the simpler model given by Eq. (1).

B.1 Model

Each cell is identified by index $i (i = 1, 2, \ldots, N)$. Let m_i, y_i, z_i, u_i, and w_i be the concentration of *her* mRNA, Her protein in cytoplasm, Her protein in nucleus, *delta* mRNA, and Delta protein in cell i, respectively. We assume that all cells have the same values of the reaction parameters. The model is:

$$\frac{dm_i}{dt} = \frac{r_1^n}{r_1^n + z_i^n}\left(r_2 + r_3\hat{w}_i\right) - \frac{r_5 m_i}{r_4 + m_i}, \tag{B.1a}$$

$$\frac{dy_i}{dt} = r_6 m_i - \frac{r_8 y_i}{r_7 + y_i} - r_9 y_i, \tag{B.1b}$$

$$\frac{dz_i}{dt} = r_9 y_i - \frac{r_{11} z_i}{r_{10} + z_i}, \tag{B.1c}$$

$$\frac{du_i}{dt} = r_{13}\frac{r_{12}^h}{r_{12}^h + z_i^h} - \frac{r_{15} u_i}{r_{14} + u_i}, \tag{B.1d}$$

$$\frac{dw_i}{dt} = r_{16} u_i - \frac{r_{18} w_i}{r_{17} + w_i}. \tag{B.1e}$$

Eqs. (B.1a)–(B.1c) are same as Eqs. (1a)–(1c).

Equation (B.1d) describes the time evolution of *delta* mRNA. The first term represents the transcription of *delta* mRNA. Her protein in nucleus represses the transcription (Horikawa et al. 2006). The second term represents degradation of *delta* mRNA.

Equation (B.1e) describes the time evolution of Delta proteins expressed on the cell membrane. The first term represents the translation of Delta protein and the second term represents its degradation.

The value of each parameter in Eqs. (B.1a)–(B.1c) was chosen from the same range of the corresponding parameter in Eqs. (1a)–(1c). Each parameter in Eqs. (B.1d) and (B.1e) was chosen from the range of its *her* counterpart. We examined Eq. (B.1) with $n = h = 1, 2, 3,$ and 4 separately and confirmed that the results depend very little on the value of the Hill coefficient. Hence, we summarize here the results for the case of $n = h = 2$.

We examined the parameter dependence of the stability of synchronized oscillation by the same methods described in the main text: we searched for a limit cycle with a period of 25–35 min in Eq. (B.1) under the constraints $m = m_1 = \cdots = m_N$, $y = y_1 = \cdots = y_N$, $z = z_1 = \cdots = z_N$, $u = u_1 = \cdots = u_N$, and $w = w_1 = \cdots = w_N$. If a limit cycle existed, we solved Eq. (B.1) under the above constraints for $3^5 = 243$ different initial conditions (procedures to generate these initial conditions were the

same as those described in Sect. 3.1 in the main text) to check whether or not the limit cycle was the only attractor in the constrained system. In 75% of 10,000 parameter sets, the limit cycle was the only attractor. Then we studied the linear stability of the limit cycle. In the system with cells aligned linearly ($N = 2, 4, 6$ and 8), we used the procedures described in Sect. 3.2, whereas in the two-dimensional case, we used the procedures in Sect. 3.3.3.

B.2 Results

B.2.1 Two-cell system

Among 7,478 parameter sets with which Eq. (B.1) had synchronized oscillation, it was stable with 1,263 (16.9%). Figure 6a shows the ratio of the fractions with stable synchronized oscillation when a focal parameter was large to the fractions with stable synchronized oscillation when it was small (circles with red line). The difference between these two fractions was statistically significant for all parameters except for the activation rate of *her* mRNA transcription by Delta-Notch signaling (r_3), the degradation rate of Her protein in cytoplasm (r_8), and the Michaelis constant for Delta protein degradation (r_{17}) (1% significant level by chi-square test). The synchronized oscillation was more likely to be stable if the basal transcription rates of *her* mRNA (r_2), the Michaelis constant for *her* mRNA degradation (r_4), the translation rate of Her protein (r_6), the threshold constant for the suppression of *delta* mRNA transcription by Her protein (r_{12}), the degradation rate of *delta* mRNA (r_{15}), and the degradation rate of Delta protein (r_{18}) were large (Fig. 6a).

In contrast, the synchronized oscillation tended to be stable if the degradation rate of *her* mRNA (r_5), the transcription rate of *delta* mRNA (r_{13}), the Michaelis constant for *delta* mRNA degradation (r_{14}), and the translation rate of Delta protein (r_{16}) were small (Fig. 6a). Smaller values of the threshold constant for the suppression of *her* mRNA transcription by Her protein (r_1), the Michaelis constant for Her protein degradation in cytoplasm (r_7) and nucleus (r_{10}), the transport rate of Her protein (r_9), and the degradation rate of Her protein in nucleus (r_{11}) also favored stable synchronized oscillation, but their influences on stability were relatively weak compared with the above four parameters.

B.2.2 N cells aligned linearly

We examined the cases in which N cells were linearly aligned ($N = 4, 6, 8$), and confirmed that the results for these systems were very similar to those for the two-cell system (Fig. 6b). Hence, we concluded that results derived from the two-cell system also hold for N cells aligned linearly.

B.2.3 N cells on a two-dimensional lattice

As in Sect. 3.3.3, we first analyzed the parameter dependence of stability in the one-dimensional models by both methods—by calculating the eigenvalues of the

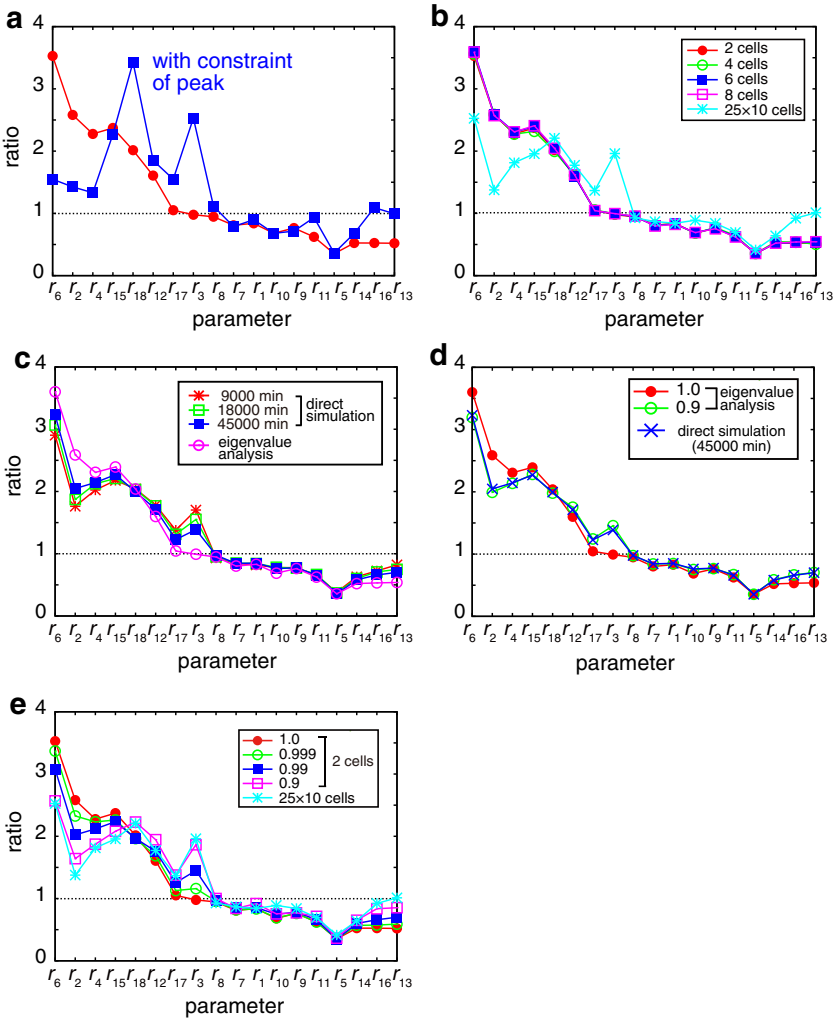

Fig. 6 **a** Ratio of the fractions showing stable synchronized oscillation when the focal parameter was large to the fractions showing stable synchronized oscillation when it was small, with (*squares*) or without (*circles*) a constraint on peak concentration. $n = h = 2$ in Eq. (B.1). **b** Results for different cell numbers: $N = 2, 4, 6, 8$ (linearly aligned), and 25×10 (two-dimensional lattice). The vertical axis is the ratio of fractions showing stable synchronized oscillation when the focal parameter was large to those when it was small. **c** Comparison between the eigenvalue analysis (*pink open squares*) and direct computer simulation results. Calculation periods for the direct computer simulations were 9,000 min (*red crosses*), 18,000 min (*green open squares*) and 45,000 min (*blue filled squares*). $N = 6$ (linearly aligned). **d** Convergence speed explains the different results between the eigenvalue analysis and the direct computer simulation (*blue crosses*). In the eigenvalue analysis, we regarded a synchronized oscillation as "stable" if the maximum eigenvalue of the fundamental solution matrix was smaller than 1.0 (*red filled circles*) or 0.9 (*green open circles*). The calculation period for the direct computer simulations was 45,000 min. $N = 6$ (linearly aligned). **e** Convergence speed explains the differences in the results between the one-dimensional models and the two-dimensional model. In the eigenvalue analysis, we regarded a synchronized oscillation as "stable" if the maximum eigenvalue of the fundamental solution matrix was smaller than 1.0 (*red filled circles*), 0.999 (*green open circles*), 0.99 (*blue filled squares*), or 0.9 (*pink open squares*). In the eigenvalue analysis, $N = 2$. We plotted the results for the two-dimensional model (25×10 cells) with Eq. (B.1) (*light blue crosses*)

fundamental solution matrix around the limit cycle and by examining the phase differences between the cells by direct computer simulation. We confirmed that these two methods gave the same results for most parameters in Eq. (B.1) (Fig. 6c). In a small fraction of the cases, direct computer simulations gave clearer results of the parameter dependence of the stability than examining the eigenvalues did in the Eq. (B.1) analysis. However, there was no case in which the difference in dependence resulted in a change of sign (Fig. 6c).

We clarified, by eigenvalue analysis, that the differences between the two methods were related to the convergence speed to the limit cycle (Fig. 6d). In the direct computer simulation, even if a limit cycle is stable it tends to be regarded as "unstable" if the convergence speed to the limit cycle is very slow, because of the finite calculation period of the computer simulation. In such a limit cycle, one of the eigenvalues of the fundamental solution matrix might be very close to one, causing slow convergence to the limit cycle. To check whether we could reproduce the results obtained by direct computer simulations by considering the convergence speed, we determined a threshold value (0.9) for the maximal eigenvalue of the fundamental solution matrix. If the maximal eigenvalue was smaller than 0.9, we regarded the synchronized oscillation as "stable" (fast convergence). If not, we regarded it as "unstable" (slow convergence or actually unstable). Because the fundamental solution matrix always has one eigenvalue equal to 1 (Niwa 1995), we excluded that eigenvalue when we assessed the maximal eigenvalue. With this constraint on convergence speed, we were able to reproduce the results obtained by direct computer simulations (Fig. 6d).

The results for the two-dimensional model with Eq. (B.1) are generally speaking similar to that for the one-dimensional model (Fig. 6b). When there was a difference, the magnitude of the dependence changed but in no case did the sign of the influence change. We confirmed by the eigenvalue analysis described above that these differences between one-dimensional and two-dimensional cases were due to the convergence speed to the limit cycle (Fig. 6e).

B.3 Constraint of concentration of molecules at the peak

In the analyses explained above we considered only a constraint on the period of oscillation (25–35 min) when we sampled parameter sets from the ranges listed in Table 1. However, there might be other constraints we should consider such as the actual concentrations of the molecules at the oscillation peak. Here, we study the parameter dependence of stability when the concentrations at the oscillation peak are constrained.

We sampled parameter sets with which Eq. (B.1) had synchronized oscillation with a period of 25–35 min and with the oscillation peak of each variable exceeding 0.1 nM. If the diameter of a cell is assumed to be 10 μm (cell volume, 524 μm^3), 0.1 nM of a molecule corresponds to about 30 copies of the molecule in the cell. We considered that it is biologically unrealistic for the oscillation of a molecule to be sustained when the copy number of a molecule is smaller than 30. Hence, we chose 0.1 nM as a biologically plausible threshold level. We examined a two-cell system ($N = 2$) with a

Hill coefficient of two ($n = h = 2$ in Eq. (B.1)). We analyzed the stability of limit cycles by the methods described in Sect. 3.2.

When we added the above constraint on peak concentration, the fraction of stable synchronized oscillation was 5.45% (484/8,877), which is smaller than the fraction when we did not consider that constraint (16.9%). The difference between the two fractions was statistically significant for all parameters except for the threshold constant for suppression of *her* mRNA transcription by Her protein (r_1), the Michaelis constant for Her protein degradation in cytoplasm (r_7), the degradation rate of Her protein in cytoplasm (r_8), the degradation rate of Her protein in nucleus (r_{11}), the *delta* mRNA transcription rate (r_{13}), and the translation rate of Delta protein (r_{16}) (1% significant level by chi-square test) (squares with blue line in Fig. 6a). Larger values of the activation rate of *her* mRNA transcription by Delta-Notch signaling (r_3) and the Michaelis constant for Delta protein degradation (r_{17}) favored stable synchronized oscillation and had a stronger influence on stability than they did in the system without any constraint on peak concentrations (Fig. 6a). The dependence on other parameters was almost same as that in the system without any constraint on peak concentrations.

References

Baker RE, Schnell S, Maini PK (2006) A mathematical investigation of a Clock and Wavefront model for somitogenesis. J Math Biol 52:458–482

Barrio M, Burrage K, Leier A, Tian T (2006) Oscillatory regulation of Hes1: Discrete stochastic delay modelling and simulation. PLoS Comput Biol 2(9):e117

Bessho Y, Miyoshi G, Sakata R, Kageyama R (2001) Hes7: a bHLH-type repressor gene regulated by Notch and expressed in the presomitic mesoderm. Genes Cells 6:175–185

Cinquin O (2007) Repressor dimerization in the zebrafish somitogenesis clock. PLoS Comput Biol 3(2):e32

Collier JR, Monk NA, Maini PK, Lewis JH (1996) Pattern formation by lateral inhibition with feedback: a mathematical model of delta-notch intercellular signalling. J Theor Biol 183:429–446

Collier JR, Mcinerney D, Schnell S, Maini PK, Gavaghan DJ, Houston P, Stern CD (2000) A cell cycle model for somitogenesis: mathematical formulation and numerical simulation. J Theor Biol 207:305–316

Cooke J, Zeeman EC (1976) A clock and wavefront model for control of the number of repeated structures during animal morphogenesis. J Theor Biol 58:455–476

Dubrulle J, Pourquie O (2002) From head to tail: links between the segmentation clock and antero-posterior patterning of the embryo. Curr Opin Genet Dev 12:519–523

Giudicelli F, Ozbudak EM, Wright GJ, Lewis J (2007) Setting the tempo in development: an investigation of the zebrafish somite clock mechanism. PLoS Biol 5(6):e150

Goldbeter A, Pourquie O (2008) Modeling the segmentation clock as a network of coupled oscillations in the Notch, Wnt and FGF signaling pathways. J Theor Biol 252:574–585

Hirata H, Yoshiura S, Ohtsuka T, Bessho Y, Harada T, Yoshikawa K, Kageyama R (2002) Oscillatory expression of the bHLH factor Hes1 regulated by a negative feedback loop. Science 298:840–843

Holley SA, Geisler R, Nusslein-Volhard C (2000) Control of her1 expression during zebrafish somitogenesis by a delta-dependent oscillator and an independent wave-front activity. Genes Dev 14:1678–1690

Holley SA, Julich D, Rauch GJ, Geisler R, Nusslein-Volhard C (2002) her1 and the notch pathway function within the oscillator mechanism that regulates zebrafish somitogenesis. Development 129:1175–1183

Honda H, Tanemura M, Yoshida A (1990) Estimation of neuroblast numbers in insect neurogenesis using the lateral inhibition hypothesis of cell differentiation. Development 110:1349–1352

Honda H, Tanemura M, Yoshida A (2000) Differentiation of wing epidermal scale cells in a butterfly under the lateral inhibition model—appearance of large cells in a polygonal pattern. Acta Biotheor 48:121–136

Horikawa K, Ishimatsu K, Yoshimoto E, Kondo S, Takeda H (2006) Noise-resistant and synchronized oscillation of the segmentation clock. Nature 441:719–723

Jaeger J, Goodwin BC (2002) Cellular oscillators in animal segmentation. In Silico Biol 2:111–123
Jiang YJ, Aerne BL, Smithers L, Haddon C, Ish-Horowicz D, Lewis J (2000) Notch signalling and the synchronization of the somite segmentation clock. Nature 408:475–479
Jouve C, Palmeirim I, Henrique D, Beckers J, Gossler A, Ish-Horowicz D, Pourquie O (2000) Notch signalling is required for cyclic expression of the hairy-like gene HES1 in the presomitic mesoderm. Development 127:1421–1429
Kaern M, Menzinger M, Hunding A (2000) Segmentation and somitogenesis derived from phase dynamics in growing oscillatory media. J Theor Biol 207:473–493
Kerszberg M, Wolpert L (2000) A clock and trail model for somite formation, specialization and polarization. J Theor Biol 205:505–510
Kobayashi R, Tero A, Nakagaki T (2006) Mathematical model for rhythmic protoplasmic movement in the true slime mold. J Math Biol 53:273–286
Kuramoto Y (1984) Chemical oscillations, waves, and turbulence. Springer, Berlin
Kurosawa G, Iwasa Y (2002) Saturation of enzyme kinetics in circadian clock models. J Biol Rhythms 17:568–577
Lewis J (2003) Autoinhibition with transcriptional delay: a simple mechanism for the zebrafish somitogenesis oscillator. Curr Biol 13:1398–1408
Mara A, Schroeder J, Chalouni C, Holley SA (2007) Priming, initiation and synchronization of the segmentation clock by deltaD and deltaC. Nat Cell Biol 9:523–530
Maroto M, Dale JK, Dequeant ML, Petit AC, Pourquie O (2005) Synchronised cycling gene oscillations in presomitic mesoderm cells require cell-cell contact. Int J Dev Biol 49:309–315
Masamizu Y, Ohtsuka T, Takashima Y, Nagahara H, Takenaka Y, Yoshikawa K, Okamura H, Kageyama R (2006) Real-time imaging of the somite segmentation clock: revelation of unstable oscillators in the individual presomitic mesoderm cells. Proc Natl Acad Sci USA 103:1313–1318
Meinhardt H (1982) Models of biological pattern formation. Academic, New York
Meinhardt H (1986) Somites in developing embryos. In: Bellairs R, Edie DA, Lash JW (eds) Nato ASI Series A, vol 118. Plenum Press, New York, pp 179–189
Niwa T (1995) An introduction to the theory of differential equations and dynamical systems. Yuseisya, Tokyo
Oates AC, Ho RK (2002) Hairy/E(spl)-related (Her) genes are central components of the segmentation oscillator and display redundancy with the Delta/Notch signaling pathway in the formation of anterior segmental boundaries in the zebrafish. Development 129:2929–2946
Owen MR, Sherratt JA (1998) Mathematical modelling of juxtacrine cell signalling. Math Biosci 153:125–150
Ozbudak EM, Lewis J (2008) Notch signalling synchronizes the zebrafish segmentation clock but is not needed to create somite boundaries. PLoS Genet 4(2):e15
Palmeirim I, Henrique D, Ish-Horowicz D, Pourquie O (1997) Avian hairy gene expression identifies a molecular clock linked to vertebrate segmentation and somitogenesis. Cell 91:639–648
Riedel-Kruse IH, Muller C, Oates AC (2007) Synchrony dynamics during initiation, failure, and rescue of the segmentation clock. Science 317:1911–1915
Rodriguez-Gonzalez JG, Santillan M, Fowler AC, Mackey MC (2007) The segmentation clock in mice: interaction between the Wnt and Notch signalling pathways. J Theor Biol 248:37–47
Rudge T, Burrage K (2008) Effects of intrinsic and extrinsic noise can accelerate juxtacrine pattern formation. Bull Math Biol 70:971–991
Saga Y, Takeda H (2001) The making of the somite: molecular events in vertebrate segmentation. Nat Rev Genet 2:835–845
Tanemura M, Honda H, Yoshida A (1991) Distribution of differentiated cells in a cell sheet under the lateral inhibition rule of differentiation. J Theor Biol 153:287–300
Tiedemann HB, Schneltzer E, Zeiser S, Rubio-Aliaga I, Wurst W, Beckers J, Przemeck GKH, Hrabede Angelis M (2007) Cell-based simulation of dynamic expression patterns in the presomitic mesoderm. J Theor Biol 248:120–129
Uriu K, Morishita Y, Iwasa Y (2009) Traveling wave formation in vertebrate segmentation. J Theor Biol 257:385–396
Winfree AT (2000) The geometry of biological time. Springer, New York
Wu Z, Yamaguchi Y (2004) Input-dependent learning rule for the memory of spatiotemporal sequences in hippocampal network with theta phase precession. Biol Cybern 90:113–124
Zeiser S, Muller J, Liebscher V (2007) Modeling the Hes1 oscillator. J Comput Biol 14:984–1000